RESEARCH ARTICLE

Infrared spectrometric biomarkers for ulcerative colitis screening using human serum samples

Hemendra Ghimire[1] | Emilie Viennois[2] | Xinjie Hu[3] | Gengsheng Qin[3] | Didier Merlin[2,4] | A. G. Unil Perera[1*] ○

[1]Department of Physics and Astronomy, Georgia State University, Atlanta, GA, USA

[2]Institute for Biomedical Sciences, Digestive Disease Research Group, Georgia State University, Atlanta, GA, USA

[3]Department of Mathematics and Statistics, Georgia State University, Atlanta, GA, USA

[4]Atlanta Veterans Affairs Medical Center, Decatur, GA, USA

*Correspondence
A. G. Unil Perera, Department of Physics and Astronomy, Georgia State University, Atlanta, Georgia 30303, USA.
Email: uperera@phy-astr.gsu.edu

Abstract

This study uses infrared spectrometry coupled with data analysis techniques to understand colitis-induced alterations in the molecular components of serum samples. Using samples from 18 ulcerative colitis patients and 28 healthy volunteers, we assessed features such as absorbance values at wavenumbers of 1033 and 1076 cm^{-1}, and the ratios at 1121 versus 1020 cm^{-1} and 1629 versus 1737 cm^{-1}. Through the deconvolution of the amide I band, protein secondary structure analysis was performed. Colitis-induced alterations are reflected as fluctuations in the vibrational modes, and are used to identify associated spectral signatures. The results of the study show statistically significant differences in five identifying spectral signatures. Among them, the sensitivity and specificity of the spectral signature, I_{1121}/I_{1020}, were 100% and 86%, respectively. These findings resemble our earlier proof-of-concept investigations in mouse models and provide preliminary evidence that this could be a reliable diagnostic test for human patients.
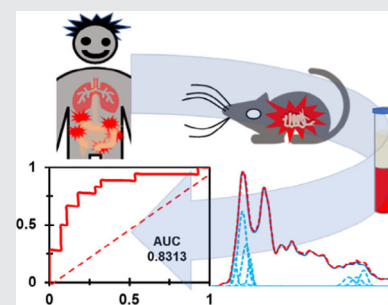
KEYWORDS
human patients, inflammatory bowel diseases, serum samples, spectral signatures, ulcerative colitis

1 | INTRODUCTION

Clinically defined inflammatory bowel disease (IBD) [1], ulcerative colitis (UC) and Crohn's disease (CD), affect the quality of life through chronic, relapsing, immunologically mediated gastrointestinal (GI) disorders [2]. The incidence and prevalence rates [3] of these diseases with unknown etiology [4] have been increasing globally. Groundbreaking advances in the understanding of these diseases [5] have been achieved using human and animal models of intestinal inflammation, but we still lack a reliable screening test with which primary care

physicians can diagnose these illnesses, and start the early administration of therapeutic strategies [6]. At present, gold standard techniques such as colonoscopy, sigmoidoscopy and small bowel follow-through are recommended for colorectal and GI diseases [7], including IBD. However, these gold-standard tests are expensive and invasive, with associated risks, and are not comfortable to use, affecting the compliance rate [8]. Studies have shown that the onset of IBD typically occurs in the second and third decades of life [9], and thereafter progresses to episodes of relapse and remission in the GI tract. In the absence of early detection,

IBD can lead to life-threatening complications including colitis-associated cancers (CACs). The colorectal cancer (CRC) awareness foundation indicates that the risk of CRC in those younger than 50 increases by 2% every year. Therefore, we critically need to develop an affordable, sensitive, specific, user-friendly, robust, and rapid, equipment-free, and deliverable (ASSURED) screening test to end-users for IBD.

Blood and its component-based biomarkers [10] have been previously studied in this context, and gene panels have been used to predict and discriminate IBD disease activity [11]. Analysis of gene panels in blood could help expand our understanding of the underlying involvement of these genes [11] and/or facilitate the development of personalized medicine [12]. However, gene expression analysis requires specific and often complicated experimental protocols and data processing techniques [10–12], and thus cannot currently be used as a rapid, low-cost and easy early screening test.

This study explores the use of attenuated total reflection Fourier transforms infrared (ATR-FTIR) spectroscopy [13] on serum samples from UC patients, building on our earlier studies in mouse models [14–17]. In ATR-FTIR spectroscopy, light is totally reflected inside the ATR crystal [18] and creates an evanescent wave that penetrates into the sample [19]. The penetration depth can be adjusted by using crystals with different refractive indices and incident angles. During decay, the loss of energy will occur at the same frequency as the sample's absorption for soft biological materials [20, 21]. Serum, which is the protein-rich blood component that remains [22] after cells and clotting factors are removed from a whole-blood sample [23], is used in numerous diagnostic tests [24, 25]. Thus, ATR-FTIR spectroscopy of serum is simple, and its use as a screening tool before colonoscopy could offer a radical alterative to standard practices for IBD diagnostics.

2 | MATERIALS AND METHODS

Human sera were purchased from Equitech-Bio, Inc. (Kerrville, TX) and stored at -80°C until analysis. The sample handling and measurement methods were carried out in accordance with relevant guidelines and regulations. Instrumentation, measurements and analysis also follow the standard protocols [13, 17]. In this study, parameters like; effect of air drying of serum samples, measurement-to-measurement and user-to-user reproducibility are also evaluated to understand the feasibility of technique in the clinical domain (Note S1:, Figure S1 for the effect of air drying and Figure S2 for

measurement-to-measurement and user-to-user reproducibility). Similarly, the detailed information about the samples are provided in Note S5 (Table S2 for UC patients and Table S3 for Controls).

2.1 | FTIR spectrometer

All the spectral data were obtained with the use of a Bruker Vertex-70 FTIR spectrometer having a KBr beam splitter and Deuterated Tri-Glycine Sulfate (DTGS) detector. An MVP-Pro ATR accessory fitted with a diamond crystal configured to have a single reflection was used. Diamond has a smaller acceptance angle cone, allowing an optical design to extract good spectra (Note S2: Figure S3). Medium Blackman-Harris apodization function was employed with a resolution of 4 cm^{-1} and a zero-filling factor of four to provide the best resolution ability (maximum signal-to-noise ratio). The aperture size is set to 2.5 mm for the optimization of the detector response without saturation.

2.2 | Spectral measurements

The ATR crystal surface was first cleaned using sterile phosphate buffered saline, and ethanol to get rid of staining substances. A cleanliness test was then conducted to ensure that the absorbance spectrum obtained without a sample had no peaks in the signal higher than the noise level. A background measurement was performed prior to each spectral measurement by scanning the cleaned crystal surface and then subtracting it from the sample signal spectrum. In each measurement, 1 µl of the sample was deposited and allowed to settle at room temperature, before taking multiple scans to get high-quality, reproducible spectra. Each sample was scanned multiple times (within $400-4000 \text{ cm}^{-1}$) to get eight or more, high-quality spectra. The last six reads of the 100 co-added scans for each sample (total 600 scans) were averaged for further statistical analysis.

2.3 | Spepectral analysis

In the course of spectral analysis, using OPUS 6.5 software, vector normalized second derivatives spectra and the min–max normalized [13] absorbance data within the region, $900-1800 \text{ cm}^{-1}$ were used. The Student's t test (with two-tailed unequal variance) p values were calculated to find prominent, discriminatory regions. The spectral signatures are then identified and quantified by comparing absorbance values, ratios and by

using spectral deconvolutins. The discriminating potential of identifying spectral signatures were further analyzed with statistical measures such as sensitivity, specificity and the receiver operating characteristic (ROC) curves [26]. The Youden index was used to find the optimal cutoff values. These cutoff values are then used to estimate the sensitivity, specificity, false positive and false negative rates. Statistical measures [27] of the discriminatory signatures reveals the usefulness of the presented diagnostic regimen. The ROC curves are plotted to find the area under the curve (AUC); for each of these features.

3 | RESULTS AND DISCUSSION

3.1 | Discrimination of absorbance values

Figure 1A shows average min–max normalized [13] infrared absorption spectra of sera covering the 900–1800 cm^{-1} region from control ($n = 28$) and UC patients ($n = 18$). This region is comprised of biological functional groups of lipids, proteins, nucleic acids and carbohydrates as assigned. The details of the normalized absorption spectra and corresponding quantified information are provided in supporting information file (Figure S4 and Tables S2 and S3). The spectral difference (UC - Control), as shown by solid green line (—) of Figure. 1B, is significantly higher than the difference obtained from the multiple measurements of the same Control (— — dashed lines) and UC (••• dotted lines) samples. Figure. 1C shows the p values for the absorbance. p values less than the nominal significance level of 0.05 indicate the discriminatory features of the spectrum. p values <0.025 are also highlighted by a pink trace line (— —). The prominent, discriminatory regions include C=O/C–N stretching and N-H bends in amides, C=O in stretching lipids, RNA/DNA nucleotides and C–O vibrations of carbohydrates [28]. Because of the complexity of biological systems, biomolecular and bonding vibration assignments are tentative and are based on numerous studies [29–31]. The spectral region, 1700–1750 cm^{-1}, is primarily recognized by its C=O stretching band in lipids [30, 31]. The amide I (1600–1700 cm^{-1}) vibration is known to be sensitive to the secondary structure of proteins [15, 29], which mainly arises due to C=O stretching vibration with minor contributions from out-of-phase C–H stretching vibrations, C–C–N deformation and N–H in-plane bends. Spectral band around 1578 cm^{-1} is due to C=N adenine [30] while the region 1136–1153 cm^{-1} is due to the ring vibration mode of C–O–C including C–O–H, C–O and C–C stretch [32]. The spectral band
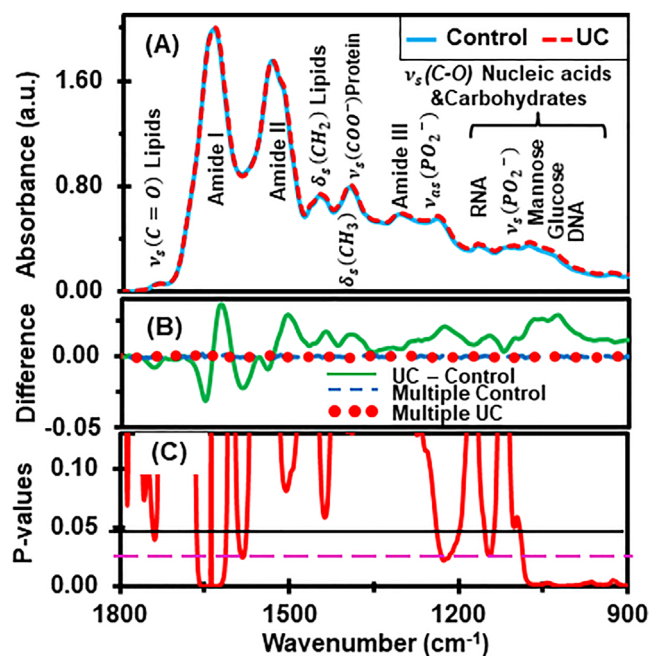

FIGURE 1 Infrared absorption spectra of sera from control and UC patients. (A) Averages min-max normalized absorbance spectra of Control ($n = 28$) and UC patients' ($n = 18$) serum samples. (B) The spectral response difference between UC and control. Average absorbance values of UC condition are elevated at carbohydrate and nucleic acids regions and fluctuating up and down in Amides region. The difference between repeat measurements of the same sample: Multiple Controls and Multiple UCs (shown by the — — blue-dashed and ••• red-dotted lines, respectively) are negligible compared with the difference spectra between the average UC and average control (— green; UC-Control). (C) p values comparison of absorbance values and values <0.05 are used to highlight discriminatory features. The pink-dotted line (— —) highlights p values <0.025

900–1091 cm^{-1} results from C–O, C–C stretch, C–H bend, deoxyribose/ribose DNA, RNA, $\nu s(PO_{2-})$ [32] of carbohydrates and nucleic acids.

Studies have reported that higher levels of mannose and glucose in IBD patients' serum as compared to control subjects [33]. Mannose level elevation in one of the glycoprotein fractions in the colonic mucus of UC patients was confirmed using tissue evaluation [34]. The colonic lesions, which are the characteristics of colitis can facilitate the diffusion of mannose to the circulating blood stream, thus manifesting mannose elevation in serum. Colitis-associated lipid metabolic dysfunction and the abnormal blood lipid profiles [35] and fluctuation in nucleic acids [36] are also reported. Furthermore, serological markers [10] for UC diagnosis and the discrimination between UC types are investigated [37]. The abnormalities in lipids, amino acids and energy metabolisms in the serum samples of IBD patients are seen [38].

Associations [39] between fatty acids and inflammatory cytokines or the protein abundance and the epigenetic alteration in the samples of UC patients have been also established. As such, variations in these reported serological markers [33–36] are most likely the primary reason for the UC induced changes in absorption frequencies of functional groups of constituents reflected in spectral signatures. The identifying spectral signatures presented in this study are (a) absorbance at wavenumber 1033 cm^{-1} (I_{1033}), primarily due to the presence of glucose [14] in the medium; (b) absorbance at wavenumber 1076 cm^{-1} (I_{1076}), representing the mannose level [14] as well as the presence of phosphate [31]; (c) the ratio of absorbances at wavenumber 1121 cm^{-1}, associated with RNA presence, to its value at 1020 cm^{-1}, associated with DNA presence [40] (I_{1121}/I_{1020}); (d) the ratio of absorbances at wavenumber 1629 cm^{-1}, indicating the presence of protein, to 1737 cm^{-1}, signaling the presence of lipids (I_{1629}/I_{1737}); and (e) the alteration in protein secondary structures.

3.2 | Protein secondary structure analysis

The amide I band [29], 1600–1700 cm^{-1}, has been used for the analysis of protein secondary structures [15, 17, 29, 41, 42]. The amide I band [29], is deconvoluted into six Gaussian function energy bands (GFEB) representing the side chain (~1610 cm^{-1}), β-sheet (~1630 cm^{-1}), random coil (~1645 cm^{-1}), α-helix (~1652 cm^{-1}), β-turn (~1682 cm^{-1}) and β-sheet anti-parallel (~1690 cm^{-1}) structures [15, 29, 42]. The minima of the second derivative spectra are used to approximate the position and the number of GFEB sufficient to fit the experimental curve.

Figure 2 shows a plot of the integral values of GFEB representing the α-helix and β-sheet protein secondary structures. The integral values of the α-helix components are less for UC cases, while the integral values of the β-sheet components are higher in UC as in Figure 2A,B. The average integral values of the α-helix and β-sheet components are also shown in Figure 2C and D, respectively. A significant difference between the integral ratios of the α-helix and β-sheet structures can be obtained between the control and UC groups (Figure 2E). Similarly, Table 1 shows the quantified information showing the average wavenumber position, and the GFEBs representing α-helix and β-sheet protein secondary structures. The average position of energy band representing the α-helix structure has significantly moved towards the higher wavenumber position in the UC serum.
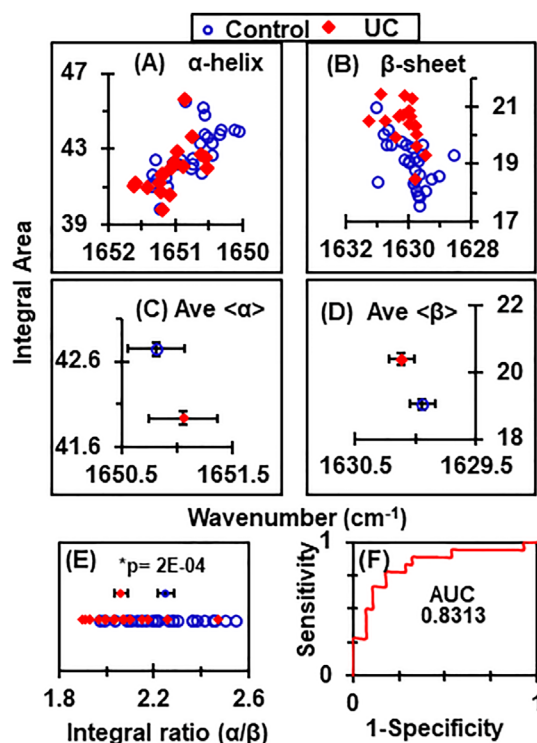

FIGURE 2 Plots of integral values of Gaussian function energy bands representing α-helix, β-sheet protein secondary structures in human sera. (A) Integral values of α-helix components. (B) The integral values of β-sheet components. (C) Average of α-helix integral values. *p* values for the integral area of α-helix is 0.05 and for their mean position is 0.03. (D) Average integral values of β-sheet. *p* values for the integral area of β-sheet is 9E-07 and their mean position is 0.3. (E) Representation of integral ratios between corresponding α-helix and β-sheet structures. Average values of control and UC cases for the integral ratio of α-helix to β-sheet (Integral [α/β]) shows a statistically significant difference. (F) The ROC curve of the Integral (α/β) and the corresponding AUC

3.3 | Identifying spectral signatures

Histogram representation of ensemble averages and the scatter plot of four spectral signatures, I_{1033}, I_{1076}, I_{1121}/I_{1020} and I_{1629}/I_{1737}, are shown in Figures 3A, B, C and D, respectively. The altered pattern between UC and control groups can be seen by comparing the range of data points and their average values in the identified spectral signatures as tabulated with standard error in the unshaded region of Table 2 (more detail are in Tables S2 and S3).

3.4 | Sensitivity and specificity

Figure 2F shows the ROC curve of the integral ratio (α/β) and the corresponding AUC. These AUC values for all the identifying spectral signatures are within 0.76–0.95.

TABLE 1 Average integral values and average positions of energy bands reflecting α-helix and β-sheet protein secondary structures

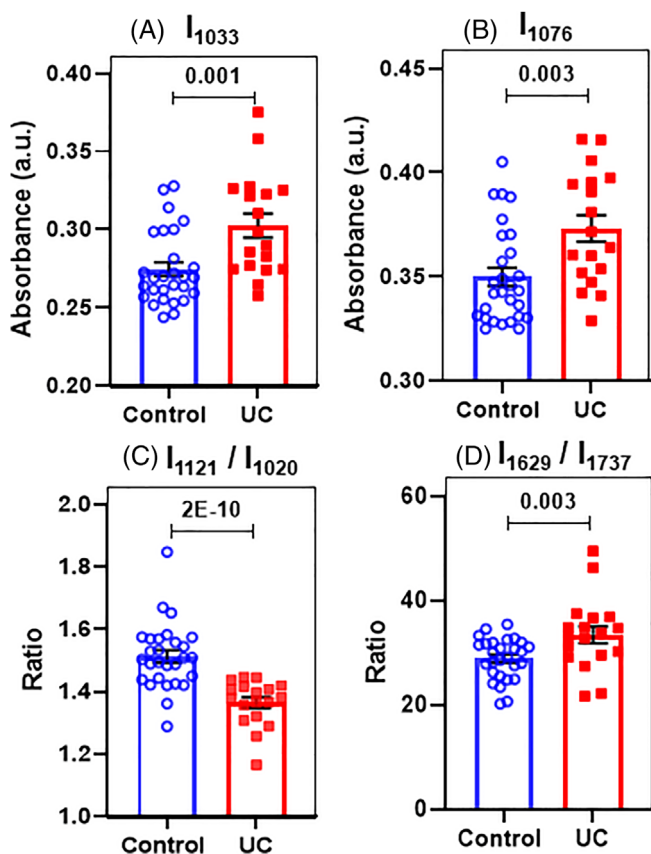| Features	Types	Integral ± SE	Difference (*p* values)	Wavenumber ± SE	Difference (*p* values)
α-helix	Control	42.74 ± 0.25	No (>0.05)	1650.81 ± 0.07	Yes (<9E-07)
	UC	41.94 ± 0.08		1651.05 ± 0.32	
β-sheet	Control	19.05 ± 0.15	Yes (<0.03)	1629.94 ± 0.11	No (>0.3)
	UC	20.40 ± 0.17		1630.12 ± 0.11	

FIGURE 3 Histogram representation of the averages of the identified spectral markers [43]. Scatter plot of data representing UC and Control samples shows the nature of variation. (A) Average absorbance values at wavenumber position 1033 cm^{-1} (I_{1033}). (B) Average absorbance values at wavenumber position 1076 cm^{-1} (I_{1076}). (C) Ratio of absorbance values (I_{1121}/I_{1020}) at wavenumber 1121 to 1020 cm^{-1}. (D) Ratio of absorbances (I_{1629}/I_{1737}) at wavenumber position 1629 to 1737 cm^{-1}. Student's *t* test, two tailed unequal variance *p* values are <0.05 in each of these identified spectral signatures. *p* values are 0.001, 0.003, 2E-10 and 0.003 for markers I_{1033}, I_{1076}, I_{1121}/I_{1020} and I_{1629}/I_{1737}, respectively

Similarly, features like optimal cutoff, AUC values, sensitivity and specificity were calculated with the aid of ROC curves are shown in the shaded region of Table 2. The maximum values of sensitivity and specificity values of each feature describe the differences between the UC versus the control groups

4 | CONCLUSION

Infrared spectral signatures were identified in UC serum samples. Identified spectral signatures include absorbance values (I_{1033} and I_{1076}), the ratio of absorbances (I_{1121}/I_{1020}, I_{1629}/I_{1737}) and the ratio of protein secondary structures (α/β). Interestingly, this study provides evidence that the ATR-FTIR spectroscopy of human serum samples resembles earlier findings using experimental mouse models [14–17]. These mouse studies also showed that the I_{1033}, I_{1076}, I_{1121}/I_{1020}, I_{1629}/I_{1737} and α/β secondary structures indicate statistically significant changes in the spectral signatures of colitis sera. The statistical measures used in the present study, such as *p* value calculations, sensitivity, specificity and ROC analysis of human samples, support the validity of the technique.

ATR-FTIR spectroscopy of body-fluids has been considered as an excellent technique to observe the biomolecular composition and their variations due to a myriad of pathologies [18]. Potential application of this technique, in the forensic sciences for the routine confirmatory screening of biological evidences is also promising [44]. The challenging aspects of the technique for its clinical feasibility, such as "measurement to measurement" and "user to user reproducibility" during the spectral measurements are also discussed (detailed discussion is presented in Note S1). The development of fully automated, user-friendly tabletop screening technique integrated with measurement and data handling approaches as discussed [13, 17] will enable the complex analysis process to the simple diagnostic decision.

Additional work is needed to further validate the spectrometric assessment of serum for IBD diagnosis and monitoring, with the goal of establishing a successful clinical technique. Using the identified spectral signatures, the required number of controls and UC cases applicable in medical diagnostic trials [45] can also be calculated (Table S1). Likewise, the impacts of parameters such as age, disease stage, sex, IBD type (UC or CD), and other comorbidities should be evaluated. Given that infrared spectroscopy of serum samples is simple, risk-free and cost-effective, we believe that this technique will be attractive to most patients for whom

TABLE 2 Quantified values of identifying discriminatory bands [43]

Types		I_{1033}	I_{1076}	I_{1121}/I_{1020}	I_{1629}/I_{1737}	Integral (α/β)
Control	Range	0.244–0.328	0.325–0.405	1.482–1.611	21.124–34.066	1.973–2.547
	Average $\pm$ SE	0.274 $\pm$ 0.004	0.349 $\pm$ 0.004	1.510 $\pm$ 0.011	28.804 $\pm$ 0.642	2.250 $\pm$ 0.030
UC	Range	0.257–0.375	0.329–0.416	1.231–1.444	22.261–48.055	1.896–2.469
	Average $\pm$ SE	0.303 $\pm$ 0.007	0.373 $\pm$ 0.006	1.362 $\pm$ 0.015	33.373 $\pm$ 1.519	2.061 $\pm$ 0.033
Cut-off value		0.273	0.351	1.446	32.815	2.099
AUC		0.782	0.762	0.944	0.762	0.831
Sensitivity (%)		89	78	100	61	78
Specificity (%)		68	68	86	93	82
p value		0.001	0.003	2E-10	0.003	0.0001

Note: Statistical measures of discriminatory infrared spectral markers for UC using sera are shown in the unshaded region. The shaded region of the table showing statistical analysis, where the optimal cut-off, and the corresponding sensitivity and specificity are calculated based on the Youden index.

routine IBD screening is recommended. Molecular mapping of infrared signatures is not expected to replace traditional colonoscopy techniques, but rather could potentially provide an additional level of information about UC patients. This is important because the early diagnosis and treatment of IBD are crucial if we hope to overcome the negative effects of these diseases on human health.

CONFLICT OF INTEREST
The authors declare no conflict of interest.

AUTHOR CONTRIBUTIONS
A. G. Unil Perera and Didier Merlin conceived the idea and designed the experiments. Hemendra Ghimire, Emilie Viennois and A. G. Unil Perera performed the spectroscopic measurements, analyzed the data, and prepared all the figures. Xinjie Hu and Gengsheng Qin performed statistical analysis. Hemendra Ghimire, A. G. Unil Perera, Emilie Viennois and Gengsheng Qin wrote the manuscript. All authors approved the final version of the article.

DATA AVAILABILITY STATEMENT
The data that support the findings of this study are available on request from the corresponding author.

ORCID
A. G. Unil Perera https://orcid.org/0000-0001-6927-7268

REFERENCES
[1] C. Fiocchi, *Gastroenterology* **1998**, *115*(1), 182.
[2] S. Lönnfors, S. Vermeire, L. Avedano, *J Crohn's Colitis* **2014**, *8*(10), 1281.
[3] C. G. Loftus, E. V. Loftus, S. W. Harmsen, A. R. Zinsmeister, W. J. Tremaine, J. L. Melton, W. J. Sandborn, *Inflamm. Bowel Dis.* **2007**, *13*(3), 254.
[4] D. K. Podolsky, *N Engl J Med* **1991**, *325*(13), 928.
[5] M. Z. Cader, A. Kaser, *Gut* **2013**, *62*(11), 1653.
[6] R. Yantiss, R. Odze, *Histopathology* **2006**, *48*(2), 116.
[7] S. Vermeire, G. van Assche, P. Rutgeerts, *Gut* **2006**, *55*(3), 426.
[8] A. R. Green, A. Peters-Lewis, S. Percac-Lima, J. R. Betancourt, J. M. Richter, M. P. R. Janairo, G. B. Gamba, S. J. Atlas, *J. Gen. Intern. Med.* **2008**, *23*(6), 834.
[9] R. Xavier, D. Podolsky, *Nature* **2007**, *448*(7152), 427.
[10] A. Tesija Kuna, *Biochem Med* **2013**, *23*(1), 28.
[11] R. Burakoff, V. Pabby, L. Onyewadume, R. Odze, C. Adackapara, W. Wang, S. Friedman, M. Hamilton, J. Korzenik, J. Levine, F. Makrauer, C. Cheng, H. C. Smith, C. C. Liew, S. Chao, *Inflamm. Bowel Dis.* **2015**, *21*(5), 1132.
[12] B. Mesko, S. Poliskal, A. Szegedi, Z. Szekanecz, K. Palatka, M. Papp, L. Nagy, *BMC Med. Genomics* **2010**, *3*(1), 15.
[13] M. J. Baker, J. Trevisan, P. Bassan, R. Bhargava, H. J. Butler, K. M. Dorling, P. R. Fielden, S. W. Fogarty, N. J. Fullwood, K. A. Heys, C. Hughes, P. Lasch, P. L. Martin-Hirsch, B. Obinaju, G. D. Sockalingum, J. Sulé-Suso, R. J. Strong, M. J. Walsh, B. R. Wood, P. Gardner, F. L. Martin, *Nat. Protoc.* **2014**, *9*(8), 1771.
[14] J. Titus, E. Viennois, D. Merlin, A. Unil Perera, *J. Biophotonics* **2017**, *10*(3), 465.
[15] J. Titus, H. Ghimire, E. Viennois, D. Merlin, A. Unil Perera, *J. Biophotonics* **2018**, *11*(3), e201700057.
[16] H. Ghimire, P. Jayaweera, A. U. Perera, *Infrared Phys Technol* **2019**, *97*, 33.
[17] H. Ghimire, X. Hu, G. Qin, A. U. Perera, *Biomed. Opt. Express* **2020**, *11*(8), 4679.

[18] S. G. Kazarian, K. A. Chan, *Analyst* **2013**, *138*(7), 1940.

[19] G. Clemens, J. R. Hands, K. M. Dorling, M. J. Baker, *Analyst* **2014**, *139*(18), 4411.

[20] M. J. Baker, S. R. Hussain, L. Lovergne, V. Untereiner, C. Hughes, R. A. Lukaszewski, G. Thiéfin, G. D. Sockalingum, *Chem. Soc. Rev.* **2016**, *45*(7), 1803.

[21] B. R. Shakya, P. Shrestha, H.-R. Teppo, L. J. Rieppo, *Appl Spectrosc Rev* **2021**, *56*(5), 347.

[22] A. G. U. Perera, H. Ghimire, in *Proc. SPIE 11236, Biomedical Vibrational Spectroscopy 2020: Advances in Research and Industry* (Eds: W. Petrich, Z. Huang), SPIE, San Francisco, CA **2020**, p. 47.

[23] E. A. Martin, Concise medical dictionary. Oxford Quick Reference, **2015**.

[24] L. L. Banez, P. Prasanna, L. Sun, et al., *J. Urol.* **2003**, *170*(2), 442.

[25] A. Lembo, B. Neri, J. Tolley, D. Barken, S. Carroll, H. Pan, *Aliment. Pharmacol. Ther.* **2009**, *29*(8), 834.

[26] A.-M. Šimundić, *EJIFCC* **2009**, *19*(4), 203.

[27] J. B. Reitsma, A. S. Glas, A. W. Rutjes, R. J. Scholten, P. M. Bossuyt, A. H. Zwinderman, *J. Clin. Epidemiol.* **2005**, *58*(10), 982.

[28] J. Ollesch, S. L. Drees, H. M. Heise, T. Behrens, T. Brüning, K. Gerwert, *Analyst* **2013**, *138*(14), 4092.

[29] H. Yang, S. Yang, J. Kong, A. Dong, S. Yu, *Nat. Protoc.* **2015**, *10*(3), 382.

[30] G. I. Dovbeshko, N. Y. Gridina, E. B. Kruglova, O. P. Pashchuk, *Talanta* **2000**, *53*(1), 233.

[31] Z. Movasaghi, S. Rehman, and D. I. ur Rehman, *Appl Spectrosc Rev*, vol. 43, no. 2, pp. 134–179, **2008**.

[32] L. Lovergne, G. Clemens, V. Untereiner, R. A. Lukaszweski, G. D. Sockalingum, M. J. Baker, *Anal. Methods* **2015**, *7*(17), 7140.

[33] R. Schicho, A. Nazyrova, R. Shaykhutdinov, G. Duggan, H. J. Vogel, M. Storr, *J Proteome Res* **2010**, *9*(12), 6265.

[34] R. Teague, D. Fraser, J. R. Clamp, *Br Med J* **1973**, *2*(5867), 645.

[35] J. Kwon, C. Lee, S. Heo, B. Kim, C.-K. Hyun, *Sci Rep* **2021**, *11*(1), 1.

[36] M. Schirmer, E. A. Franzosa, J. Lloyd-Price, et al., *Nat Microbiol* **2018**, *3*(3), 337.

[37] J. Barahona-Garrido, H. M. Sarti, M. K. Barahona-Garrido, J. Hernández-Calleros, E. Coss-Adame, S. M. Garcia-Saenz, J. K. Yamamoto-Furusho, *Rev Gastroenterol Mex* **2009**, *74*(3), 230.

[38] E. A. Scoville, M. M. Allaman, C. T. Brown, A. K. Motley, S. N. Horst, C. S. Williams, T. Koyama, Z. Zhao, D. W. Adams, D. B. Beaulieu, D. A. Schwartz, K. T. Wilson, L. A. Coburn, *Metabolomics* **2018**, *14*(1), 17.

[39] D. M. Wiese, S. N. Horst, C. T. Brown, M. M. Allaman, M. E. Hodges, J. C. Slaughter, J. P. Druce, D. B. Beaulieu, D. A. Schwartz, K. T. Wilson, L. A. Coburn, *PLoS One* **2016**, *11*(5), e0156387.

[40] R. Sahu, S. Argov, A. Salman, et al., *Technol. Cancer Res. Treat.* **2004**, *3*(6), 629.

[41] H. Ghimire, M. Venkataramani, Z. Bian, Y. Liu, A. U. Perera, *Sci. Rep.* **2017**, *7*(1), 16993.

[42] H. Ghimire, C. Garlapati, E. A. M. Janssen, U. Krishnamurti, G. Qin, R. Aneja, A. G. U. Perera, *Cancer* **2020**, *12*(7), 1708.

[43] H. M. Ghimire, Infrared Spectroscopy of Serum Samples for Disease Diagnostics, Dissertation, Georgia State University, **2021**. https://scholarworks.gsu.edu/phy_astr_diss/126.

[44] C.-M. Orphanou, *Forensic Sci. Int.* **2015**, *252*, e10.

[45] J. Cohen, *Statistical Power Analysis for the Behavioral Sciences*, 2nd ed. Academic Press, New York, **2013**.

SUPPORTING INFORMATION

Additional supporting information may be found in the online version of the article at the publisher's website.